Thin Solid Films 590 (2015) 103–110

Contents lists available at ScienceDirect

Thin Solid Films

journal homepage: www.elsevier.com/locate/tsf

Metal–organic coordinated multilayer film formation: Quantitative analysis of composition and structure

Alexandra S. Benson, Meagan B. Elinski, Monica L. Ohnsorg, Christopher K. Beaudoin, Kyle A. Alexander, Graham F. Peaslee, Paul A. DeYoung, Mary E. Anderson *

Department of Chemistry, Hope College, 35 E. 12th St., Holland, MI 49422, USA

ARTICLE INFO

Article history:
Received 19 August 2014
Received in revised form 24 June 2015
Accepted 20 July 2015
Available online 23 July 2015

Keywords:
Self-assembly
Layer-by-layer
Surface roughness
Scanning probe microscopy
Rutherford backscattering spectrometry

ABSTRACT

Metal–organic coordinated multilayers are self-assembled thin films fabricated by alternating solution–phase deposition of bifunctional organic molecules and metal ions. The multilayer film composed of α,ω-mercaptoalkanoic acid and Cu (II) has been the focus of fundamental and applied research with its robust reproducibility and seemingly simple hierarchical architecture. However, internal structure and composition have not been unambiguously established. The composition of films up to thirty layers thick was investigated using Rutherford backscattering spectrometry and particle induced X-ray emission. Findings show these films are copper enriched, elucidating a 2:1 ratio for the ion to molecule complexation at the metal–organic interface. Results also reveal that these films have an average layer density similar to literature values established for a self-assembled monolayer, indicating a robust and stable structure. The surface structures of multilayer films have been characterized by contact angle goniometry, ellipsometry, and scanning probe microscopy. A morphological transition is observed as film thickness increases from the first few foundational layers to films containing five or more layers. Surface roughness analysis quantifies this evolution as the film initially increases in roughness before obtaining a lower roughness comparable to the underlying gold substrate. Quantitative analysis of topographical structure and internal composition for metal–organic coordinated multilayers as a function of number of deposited layers has implications for their incorporation in the fields of photonics and nanolithography.

1. Introduction

A multilayer architecture of either organic (soft) or inorganic (hard) materials is a common structure for a variety of technological applications, from capacitors to photonic devices. Within the realm of organic multilayers, some common synthetic methods include polyelectrolyte assembly, dendrimeric growth, surface-initiated ring-opening metathesis polymerization, and chemical vapor deposition [1–7]. These systems have been integrated in a wide range of applications such as anti-fouling coatings or for drug delivery [8–10]. Inorganic examples of alternating layers for device architectures (*i.e.*, capacitors and multilevel flash memory) are formed by traditional processing methods such as metal evaporation, ion beam sputtering, and molecular beam epitaxy as well as by nontraditional solution-phase layer-by-layer methods [11–14]. Metal–organic coordinated multilayers are a hybrid inorganic–organic system characterized by the ability to tailor and tune thickness in the sub-nanometer scale with chemically selective deposition [15–26]. These metal–organic coordinated multilayers are simple to fabricate as they do not require high energy or vacuum systems, and they have been studied for applications in lithography, electronics, and photonics [27–40].

The metal–organic coordinated multilayer system that has been systematically characterized here is α,ω-mercaptoalkanoic acid complexed with copper (II) ions. This system was first studied by ellipsometry, followed by X-ray photoelectron spectroscopy investigations that revealed a mixture of oxidation states of the copper ions within the compositional structure [15,41]. Other key studies investigated the protonation of the terminal carboxylic acid and its impact on coordinating the copper ions [42,43]. These multilayers have application as "molecular rulers" to measure out or build up precise nanoscale lithographic resists, which can define spacings between metal features [29–32,34]. These films are often represented by a figure showing a 1:1 ratio for metal:molecule and an equal density of the additional layers relative to the base layer (Fig. 1), but the structure for this seemingly simple system has not been established unambiguously. In an effort to understand the film formation, research in the past decade has looked at this multilayer film structure and composition by scanning probe microscopy, ellipsometry, contact angle goniometry, and infrared reflection spectroscopy [44–46]. These previous studies, which focused on examining the initial few layers of the film, found a composition that was copper deficient and a topographic structure with islands formed atop underlying layers due to incomplete layer formation. Research described here

* Corresponding author.
E-mail address: meanderson@hope.edu (M.E. Anderson).

http://dx.doi.org/10.1016/j.tsf.2015.07.048
0040-6090/

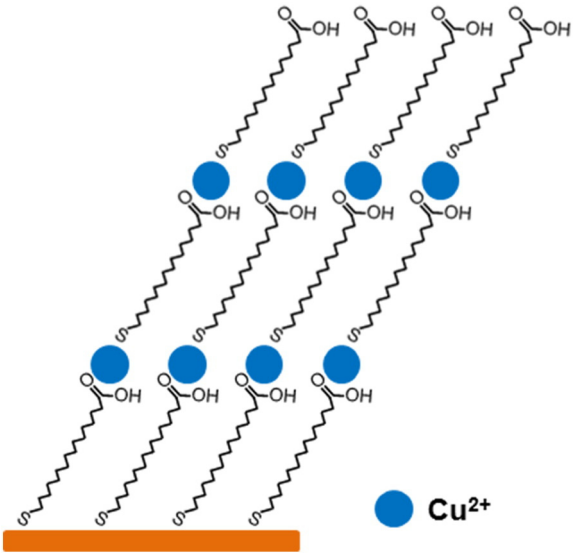

Fig. 1. Schematic representing three layers of a metal–organic coordinated multilayer thin film, composed of α,ω-mercaptoalkanoic acid and Cu^{2+} ions (blue spheres). This is the commonly accepted structure with a 1:1 ratio of metal ion to organic component [15]. (For interpretation of the references to color in this figure legend, the reader is referred to the web version of this article.).

systematically investigated foundational layers as well as thicker films to understand the physical phenomenon that underpins film growth, describing the transition from foundational layers to thicker films when the film takes on its own unique stable morphology.

In the studies presented herein, the topographical structure and the internal composition of these metal–organic coordinated multilayers have been investigated quantitatively as a function of the number of layers deposited to understand their film formation. Topographic structure has been examined by scanning probe microscopy (SPM) with a quantitative investigation of surface roughness and a qualitative observation of film morphology. This comprehensive study of layers 1–30 has allowed for the visualization of how the film morphology changes from a conformal coating mimicking the underlying substrate to a material with its own distinct structure. Films up to 30 layers in thickness have had their composition investigated by Rutherford backscattering spectrometry (RBS) and particle induced X-ray emission (PIXE). These are techniques commonly used to look at inorganic films, but are here shown to be effective for determining molecule-to-metal ion ratios and molecular film density for this hybrid inorganic–organic multilayer system [47,48].

2. Experimental details

2.1. Materials

Copper (II) perchlorate hexahydrate (98%) and 16-mercaptohexadecanoic acid [MHDA] (90%) were used as received from Aldrich (Saint Louis, MO). Absolute, anhydrous ethanol (200 proof, ACS/USP Grade) was obtained from Phamco-Aaper (Shelbyville, KY). Silicon wafers were received from Silicon Quest International (San Jose, CA) and the deposited metals of chromium and gold were purchased from Kurt J. Lesker (Jefferson Hills, PA).

2.2. Sample preparation

The multilayers were formed through bottom-up assembly by alternating solution–phase deposition between 1 mM ethanolic solutions containing MHDA or Cu (II) ions [15]. The multilayers were deposited on a gold film prepared by metal evaporation. The substrate was a silicon wafer substrate with 100 nm of thermally grown oxide and the metal film was composed of a 10 nm Cr adhesion layer followed by 100 nm Au. The first self-assembled monolayer (SAM) was grown on the gold substrate by submersion in the MHDA solution. After 1 h, the sample was removed, rinsed with ethanol, and gently dried with lab air. The sample was then submerged in the copper ion solution for 15 min, and similarly rinsed and dried. Submersion in a fresh solution of MHDA for 1 h followed by rinsing and drying completed the second layer, and this process was continued to deposit the desired number of layers. To obtain a sample set (set of 0, 1, 5, 10, *etc.* layers), the substrate was cleaved into separate samples after completion of the desired layer, and the remaining substrate was used for continued growth. In this manner, sample sets were prepared from the same gold substrate for consistency within the sample. In all cases, the terminal layer was the organic component.

2.3. Ellipsometry

To investigate linear film growth, film height was characterized *via* ellipsometry. Measurements were obtained using a variable angle discreet wavelength ellipsometer (PHE-101 VADE, Angstrom Advanced, Braintree, MA). A wavelength of 632.8 nm and a fixed angle of 70° were used to collect multiple points per substrate (for each sample, a minimum of three spots were measured). Using the PHE-102 analysis software, the film height was calculated based on refractive index values of $n = 1.5$ and $k = 0$ [15].

2.4. Contact angle goniometry (CAG)

To examine film growth by studying film hydrophobicity and surface roughness, static contact angles were obtained using an Easy Drop contact angle goniometer (Krüss, Matthews, NC). At ambient conditions, a 10 μL water droplet was delivered *via* a 500 μL syringe and flat-tipped needle. Then an image was collected to measure the angle between the droplet and the sample surface. The Kruss Drop Shape Analysis program was used to determine the contact angle. A minimum of three drops per sample were collected.

2.5. Scanning probe microscopy (SPM)

Images were obtained using a Dimension Icon Atomic Force Microscope (Bruker, Santa Barbara, CA) operating in peak force tapping mode (ScanAsyst) using etched silicon tips, and SCANASYST-AIR (Bruker, Santa Barbara, CA), with a spring constant range of 0.2–0.8 N/m and a resonant frequency range of 45–95 kHz. A minimum of three images (512 × 512 pixels) were collected for each sample and scan parameters were as follows: 1 Hz scan rate, 13.8 μm z-range, 205 mV amplitude setpoint, and 155 mV drive amplitude. Image analysis was routinely undertaken using the Nanoscope Analysis software (Bruker, Santa Barbara, CA). Matlab (MathWorks) and Image J (NIH online resource) software were also used for advanced image analysis to determine surface roughness and surface coverage, respectively.

2.6. Particle induced X-ray emission (PIXE)

To study the elemental concentration of the samples, PIXE spectrometry was performed using the Ion Beam Analysis Lab at Hope College. An ion beam of protons (H^+) accelerated to 3.4 MeV was used to irradiate each sample *in vacuo*, and the resultant X-rays were detected at 135° relative to the incident beam by a lithium-drifted silicon detector. Each sample was irradiated by several nA of beam for ~5 min per sample. A minimum of three locations across each sample were measured and the X-rays were quantified by thick-target analysis with the program GUPIXWin to determine elemental composition (in ppm) [49]. NIST-SRM calibration standards (614 and 2586) provided absolute normalization of elemental concentrations.

2.7. Rutherford backscattering spectrometry (RBS)

To study film composition and to measure areal density (atoms/cm^2), RBS was conducted using a 2.9 MeV beam of alpha particles (He^{1+}) from the Hope College Ion Beam Analysis Laboratory. Scattered alpha particles were detected in a silicon surface-barrier detector located at 168.2° relative to the beam, which was energy calibrated with a mixed alpha source. The program SIMNRA was used for data analysis to model the energy spectra obtained from the backscattered particles [50,51]. The elemental composition is determined by the precise energy measurement of the backscattered particles after their nuclear collisions with the target nuclei, and the areal density is determined by the number of backscattered particles per incident beam intensity and solid angle. For each substrate, multiple regions were sampled with an incident beam of ~5 nA for ~10 min apiece and three measurements from the same region were combined to obtain higher resolution spectra. It was also noteworthy that when the same region was repeatedly sampled there was no deviation in the result, confirming that the sample was not degraded by the particle beam.

3. Results and discussion

The structure and composition of multilayer films were studied with a particular emphasis on the surface morphology and roughness, the density of each layer (molecules/cm^2) in the film, and the concentration of copper within the film. In order to understand how these characteristics may change with increasing numbers of multilayers, sample sets were investigated for multilayer films containing a range of thicknesses from 1 to 30 layers (note the organic component is in all cases the terminal layer). To investigate how morphology and roughness change with increasing number of multilayers, ellipsometry, contact angle goniometry, and scanning probe microscopy were employed. Particle-induced X-ray emission and Rutherford backscattering spectrometry were utilized to investigate the average areal density of the individual layers and to determine the binding ratio between metal ions and molecules.

3.1. Film formation characterization by ellipsometry and contact angle goniometry

Ellipsometry data were collected, as shown in Fig. 2a, to monitor film growth. This data set is from a single piece of gold that was cleaved after iterations of approximately 5 layers until 30 layers of the film were deposited. The steady increase in film thickness, with a slope of 17 Å/layer, indicates the molecules are maintaining their alignment as an organized monolayer and not collapsing or lying flat as subsequent layers were formed. Routine multilayer film growth was shown; and no unexpected trends were observed through this characterization.

The contact angle goniometry data shown in Fig. 2b are from the same sample set (1–30 layers) as the ellipsometry data. The angles were all ~50–60° which are much lower than the unmodified gold with a contact angle greater than 100° (included as the zero-layer point on Fig. 2b). The decrease in contact angle is due to wettability differences in changing from a gold surface to a layer terminated with carboxylic acid tail groups. While copper can form complexes with sulfur and the carboxylic acid functional groups, copper has greater affinity for sulfur forming a copper thiolate leaving the carboxylic acids unbound and exposed on the surface [41,46].

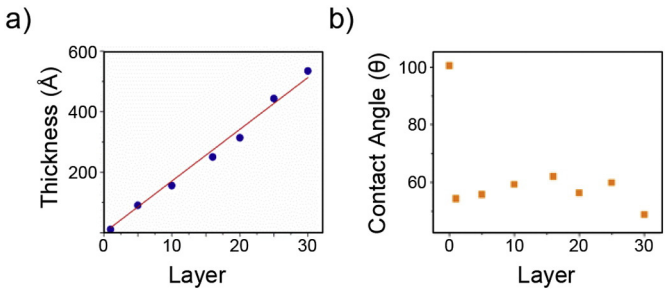

Fig. 2. a) Ellipsometry data displaying film thickness as a function of the number of layers deposited, indicating linear layer-by-layer film growth. b) Contact angle goniometry results as a function of the number of layers in the film.

3.2. Film topography characterization by scanning probe microscopy

Both thin and thick stacks of multilayers were studied in order to investigate film formation as a function of increasing layer deposition cycles. SPM images, shown in Fig. 3, were collected for single depositions of film growth up to five layers, then approximately five deposition layer increments up to thirty layers.

Images were analyzed using two different methods to determine the surface roughness of each sample. A surface roughness parameter, Rq, was found using the "Nanoscope Analysis" software and a different measure of surface roughness, Ws, was found using Matlab. These two roughness measurement numbers (Rq and Ws) are listed beneath the representative images in Fig. 3. The roughness measurement (Rq), found using the commercial image analysis software, represents the average deviation of height from the mean over the entire image area. The Ws roughness measurement is a more rigorous analysis that is able to quantitatively describe surface features (*i.e.*, grain structure size) and permits differentiation between short- and long-range roughness [52–54]. The Ws roughness number is determined as a function of area after sampling multiple "box" sizes collected for each image. For each image, fourteen box sizes are chosen to be uniformly distributed on a log scale relevant for analysis. The entire image is sampled for each box size with a single pixel step size shifting the box systematically across and down the image repeating the roughness calculation. The roughness for each box position is averaged for that box size. A curve is generated displaying the roughness as a function of box size. Specifically, the roughness (Ws) is a fit parameter representing the limit of roughness at large box sizes. Representative curves from this method are shown in Fig. 4. Shown in Fig. 5 are average Rq and Ws values for multiple images collected for films assembled with that specific number of layers. Agreement of the two different methods used to determine surface roughness was observed, as shown in Figs. 3 and 5. The calculated Ws value, obtained by the more rigorous analysis, was always equal or slightly greater than the singular Rq value obtained for the entire image area.

By quantitatively analyzing the roughness of these films in this manner, a strong correlation was observed with what could be described qualitatively by the SPM images. In the atomic force microscopy images in Fig. 3, an evolving morphology is observed in the first four layers as the film transitions to a structure that is generally maintained out to 30 layers. In the beginning as the first layer of MHDA is deposited, the underlying grains of the gold film are still observed as the film has conformally coated the underlying substrate. Upon the deposition of 2 layers, the observance of protrusions (islands) becomes apparent with some of the grains of the gold surface beneath still observed. The size of these islands increases with an increased number of depositions as is seen in the 3 layer and 4 layer images. Using Image J software to determine percent coverage of the bright protrusions (islands), it was found that the percent islands increased from 40% to 60% to 80% respectively with increasing deposition from 2 layers to 4 layers. During the increase in the size of the islands, the surface features of the underlying gold substrate become less apparent. Upon reaching five layers, a general surface structure is observed with small randomly-distributed round bulbous features; and this general structure is seen to persist for all images through the 30 layer sample.

These data suggest that the foundational layers of the film adopt the surface morphology of the underlying gold substrate with small islands protruding and increasing in size as layer deposition increases until the

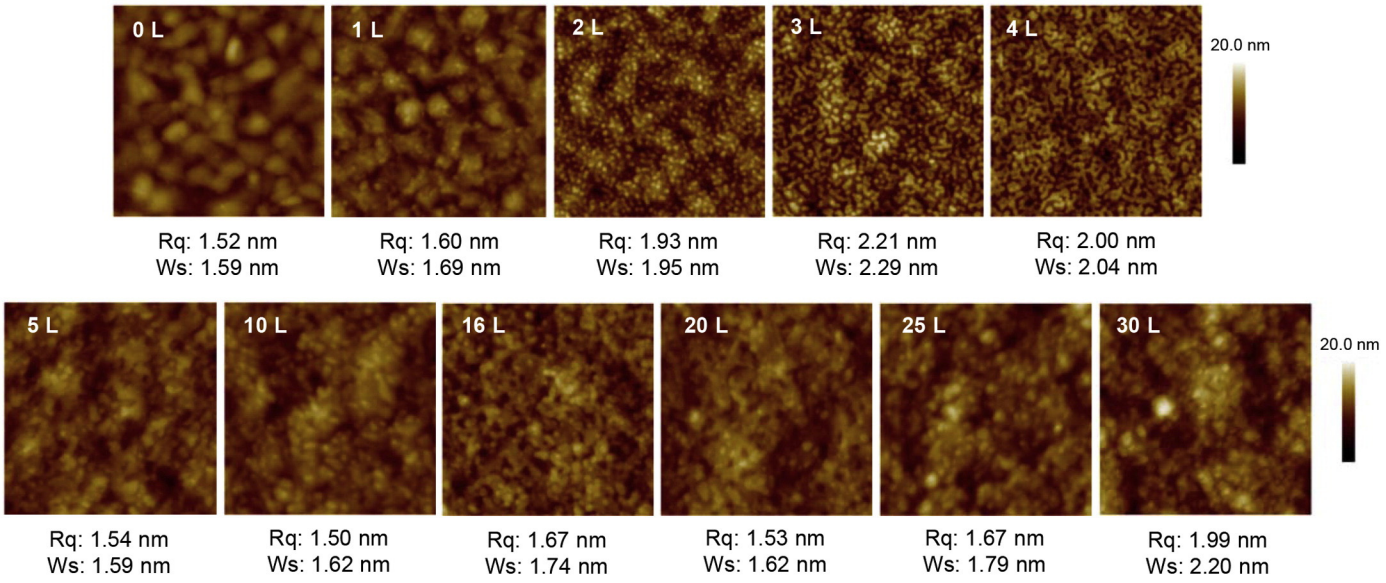

Fig. 3. Representative SPM images obtained to investigate multilayer film formation. The images are labeled with the number of layers deposited (L) and measured surface roughness (Rq, Ws) as obtained by different image analysis techniques. Each scan is 500 × 500 nm.

features of the underlying gold substrate are no longer influencing the film morphology. These islands seem to be smoothed out or "healed" as the film increases in thickness beyond five layers, suggesting that a different growth mechanism or structure may be occurring after the initial layers are formed.

Quantitatively, the change in the first foundational layers of this film is observed by the increase in the surface roughness with a peak after 3 layers of deposition. Interestingly as the growth continues for increasing numbers of layers, the roughness is consistent and on par with the roughness of the underlying gold surface (although the size of the grains or bulbous regions in the film are much smaller than the grains of the gold). Future work will investigate gold with different roughnesses to see if the same phenomenon occurs. Additionally, studies with an automated deposition tool will be used to fabricate films greater than 30 layers in thickness for roughness characterization in order to determine if the increase in surface roughness observed at 30 layers (as seen in Fig. 5) continues or is an anomaly.

While the roughness numbers (Rq) from the Nanoscope Analysis software help to glean insight as described above, the slight difference in roughness numbers between the 3 L and 30 L sample, for example, does not reflect the observed dramatic visual difference in the films. In order to explore this difference more quantitatively, the roughness as a function of area was investigated by employing Matlab. These data are shown in Fig. 4 where three different box sizes (areas) are overlaid on the images and then also highlighted in the roughness plot below. Each area on the plot represents the average roughness within that box size investigated over the entire image. Explicitly, this means that the roughness in the box in the upper left corner is calculated, then

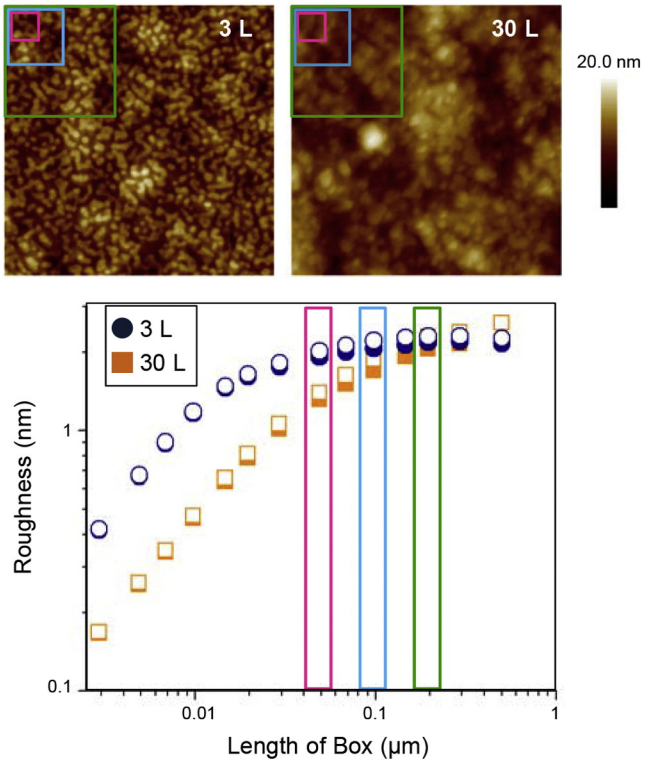

Fig. 4. Image analysis using Matlab allows for the determination of roughness (Ws) as a function of length scale. The images are labeled with the number of layers deposited (L) and boxes representing three size regimes are highlighted. Two imaged regions for each sample are graphed (empty and filled). Each image is 500 × 500 nm.

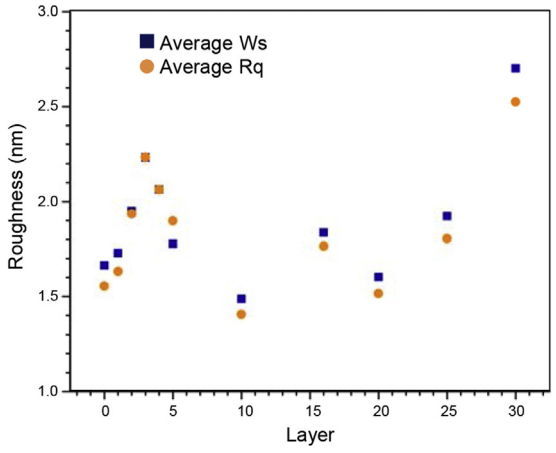

Fig. 5. Average multilayer roughness numbers as obtained by different image analysis programs, Ws and Rq.

the box is moved over one row of pixels to determine the roughness in it, and this is repeated over the entire image area.

In Fig. 4, note the difference in the curves for the different samples as it is the shape of these curves that quantitatively reflects the different morphologies. The 3 L sample has a curve that has a sharper increase in roughness indicating that it has a high degree of short-range roughness, while the 30 L sample is smoother over those short ranges. By analyzing these curves, the typical feature (grain) size can be determined [52–54]. The grain size is a fit parameter that correlates to the length of the box at which the Ws roughness becomes constant. For the 3 L image above, the average grain feature was 16 nm and for the 30 L image it was 58 nm, further emphasizing the difference between these two morphologies.

3.3. Film structure and composition characterized by ion beam analysis

These SPM data highlight a transition point in the film growth as it changes from a conformal coating of the substrate and becomes a distinct film taking on its own morphology, unique from the underlying surface features. This surface characterization expands upon previous reports that studied only the foundational layers [44–46]. XPS and IR have been used to study the composition and internal structure of those foundational layers [41–46], but are techniques that are unable to yield results for the thicker stacks. For films with 5 and more layers, PIXE and RBS are able to be employed and here have been used to determine the copper concentration in the film and molecular density in each layer. Table 1 contains a compilation of the elemental analysis results alongside the data obtained by ellipsometry, CAG, and SPM.

3.3.1. Particle induced X-ray emission

X-ray spectra, as shown in Fig. 6, were collected by PIXE. Samples were composed of a silicon wafer having a thin adhesion layer of chromium under the gold film on which the copper-coordinated multilayers were assembled. Sample components had the following X-ray lines detected: silicon (K_α = 1.73998 keV), chromium (K_α = 5.41472 keV, K_β = 5.94671 keV), gold (L_α = 9.7133 keV, L_ι = 8.4939 keV), and Cu (K_α = 8.04778 keV) [55]. These lines have all been labeled in Fig. 6. It is noteworthy that the organic component of the multilayers contained sulfur but its X-ray lines (K_α = 2.30784 keV, K_β = 2.4640 keV) were not detected due to overlap with the gold M X-rays (energy range 1.648–2.883 keV) [55]. All PIXE results were analyzed with commercial peak-fitting software GUPIXWin with the thick-target analysis mode.

Ideally with PIXE, the direct ratio of sulfur-to-copper concentrations would be compared to determine the metal-to-molecule ratio. However, due to the similarity of X-ray energies for the sulfur K lines and the abundant gold M X-rays, it was not possible to obtain a sulfur concentration. Therefore, the concentration of Cu relative to the Au substrate was measured by normalizing the Cu K_α line (8.04778 keV) to the Au L_α line (9.7133 keV) resulting in the ratio given in Table 1. This normalization accounted for variations in beam intensity between samples as is seen by the different maximum peak intensities in Fig. 6. An increase in Cu concentration was observed with an increasing number of deposited multilayers. The increase in the peak height for Cu, as a function of the number of deposited layers, can be readily observed in Fig. 6.

Table 1
Compilation of quantitative data obtained by ellipsometry, contact angle goniometry, scanning probe microscopy, particle induced X-ray emission, and Rutherford backscattering spectrometry for films having 0 to 30 deposited layers.

Layer	Thickness (Å)	Contact angle (degrees)	Rq (nm)	Ws (nm)	PIXE: Cu/Au	RBS: MHDA/cm^2 per layer
0	0	101	1.56	1.66	–	–
5	90.8	56	1.90	1.78	–	2.50E + 14
10	156	59	1.41	1.49	1.35E − 03	1.92E + 14
16	251	62	1.77	1.84	1.47E − 03	2.40E + 14
20	314	56	1.52	1.60	2.57E − 03	1.49E + 14
25	443	60	1.81	1.92	4.16E − 03	2.50E + 14
30	535	49	2.53	2.70	5.67E − 03	2.56E + 14

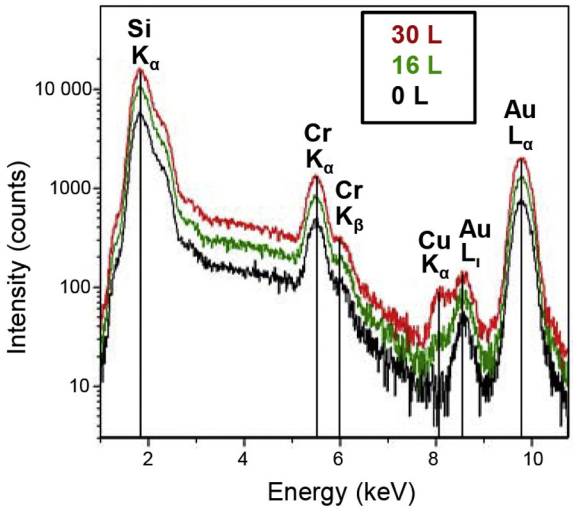

Fig. 6. Representative PIXE spectra for films composed of different numbers of layers (L) with X-ray peaks labeled according to their corresponding elements.

3.3.2. Rutherford backscattering spectrometry

Both the metal-to-molecule ratio (*i.e.*, copper ion to 16-mercaptohexadecanoic acid ratio) and the areal molecular density of the layers were determined by RBS. Energy loss spectra were obtained for samples of five to thirty layers in thickness. Representative data for the 30 layer sample are shown in Fig. 7. Multiple regions of each substrate were sampled to demonstrate uniformity across the sample and to obtain high quality statistics for analysis. The commercial fitting program SIMNRA was used to fit each spectrum, and the energy response of the detector was calibrated precisely with a mixed alpha source. The thickness (atom density) and elemental ratio were varied to fit the spectrum. Peaks resulting due to particles backscattered off the different components of the SiO_2/Cr/Au substrate were detected at 200–1700 keV, 2100 keV, and 2650 keV respectively. A shift to lower energies in the front edge of the Au peak is seen for the 30 L sample in Fig. 7c. This additional energy loss is due to the multilayer film deposited on the gold surface of the substrate; and fitting this shift permits the areal density of the film to be determined. This peak shifts to lower energies incrementally for all films sampled up to the thirty layers due to the decreased energy of the particles backscattered off the gold interface. The peak at 2335 keV arises in the multilayer films due to scattering from the incorporated Cu ions. The Cu peak intensity is found to increase relative to the other peaks for samples containing an increased number of deposited layers. The fitting of this peak involved modeling the film composition of Cu ions relative to the MHDA molecules. A variety of ratios were investigated and the ratio of 1:1, 2:1, and 3:1 are displayed on Fig. 7b. For all samples studied from 5 to 30 layers, the best fit was determined to be 2:1 suggesting that these films are copper-enriched. Table 1 displays the results of the RBS findings for the average molecular density per layer of the film (MHDA/cm^2 per layer).

The overall average molecular density per layer was found to be $2.23 \times 10^{14} \pm 4.3 \times 10^{13}$ molecules/cm^2, which is comparable to the accepted standard molecular density for a self-assembled monolayer (SAM) of 4.5×10^{14} molecules/cm^2 [56]. This result is a key finding supporting the uniformity and stability of the layers composing the structure of the multilayer film. The slightly lower density for these films is consistent with the experimental conditions for the multilayer films studied here: 1) the molecules are carboxylic acid terminated, which slightly decreases the packing density, 2) the deposition occurred for only an hour, so van der Waal interactions were not completely maximized, and 3) the underlying layer structure is not the same type

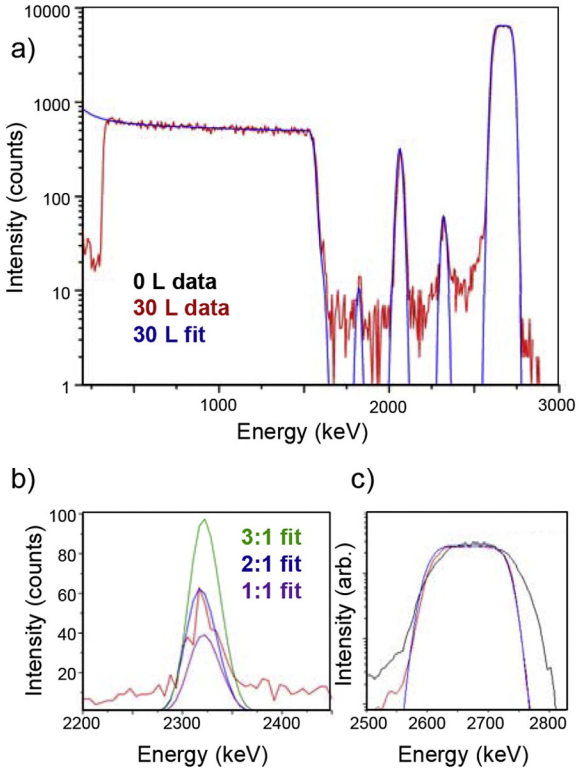

Fig. 7. Representative RBS data for the 30 layer sample. a) Logarithmic plot displaying the experimental results overlaid with the optimized fit for a thin film having a 2 copper to 1 molecule ratio. b) Linear plot of the data for the peak resulting from collisions with the copper in the film. Overlaid are three fits based on models for films composed of 1:1, 2:1, and 3:1 copper:molecule ratios. c) Logarithmic plot overlaying a spectrum for the bare Au substrate (0 L) with the 30 L sample data (experimental and calculated 2:1 fit). This portion of the spectra shows the shift in the leading Au edge to lower energy due to the presence of the thin film. The 0 L and 30 L data have been normalized.

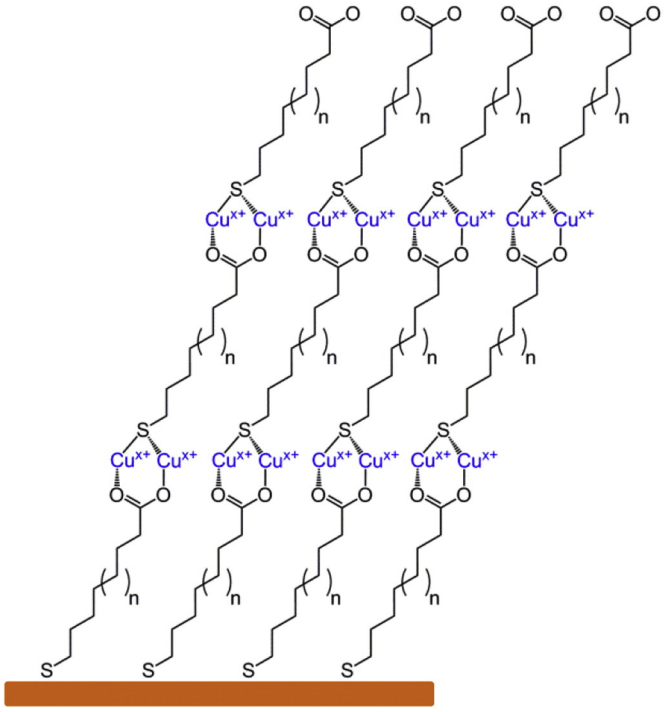

Fig. 8. Proposed chemical structure for three layers of a metal–organic coordinated multilayer thin film, composed of copper ions and α,ω-mercaptoalkanoic acid complexed with a 2:1 ratio consistent with findings herein.

of "ideal" surface commonly used for SAMs. The regularity of this layer density for multilayer films composed of an increasing number of layers, in combination with the ellipsometry data, suggests that film formation occurred in a uniform manner and that the film structure maintained an organized framework. This internal structure uniformity is consistent with the homogeneous morphology observed by SPM for films five to thirty layers in thickness

For the study of these thicker multilayer films (5–30 L), an excess of Cu ions relative to the MHDA molecules was observed. This 2:1 ratio of Cu:MHDA is in contrast to other studies that investigated bi- and tri-layer films and found them to be copper deficient with a 1:2 ratio [44,45]. This change in internal composition for the thin films to the thicker films may play a role in the external morphology transitions observed by SPM. In the SPM studies, the islands in the two, three, and four layer films seem to be smoothed out or healed as the film increases in thickness beyond five layers. This suggests that a different growth mechanism or structure is occurring after the initial layers are formed — one that does result in the formation of continuous layers being created after each deposition cycle. This increase in copper concentration is hypothesized to be essential in the film structure being smoothed out and taking on its own unique morphology apart from the underlying substrate; hence the increased incorporation of copper may allow for the layer-by-layer growth to occur uniformly for the multilayers deposited after the foundational layers are established.

The thicker films (>5 layers) are shown by ellipsometry, SPM, PIXE, and RBS to be uniform in layer thickness, external morphology, elemental composition, and molecular density. These data suggest that each molecule has two copper ions complexed at the metal–organic interface, supporting subsequent ordered layer formation at the same density as the one underlying it (Fig. 8). This type of coordination is uncommon and seems unsatisfactory from a charge-balance perspective. However, this data may in part be explained by recent findings regarding the reduction of the Cu (II) to Cu (I) after the deposition of the organic layer and the change in conformation of the top organic layer upon the formation of the complex between the Cu (II) ions and the surface carboxylates [46]. It could be hypothesized that during the complexation of ions on the exposed carboxylates, that additional ions are also being incorporated at the underlying interface where copper (I) thiolates have been formed. The conformational change could be induced by the densification of the underlying copper layer. Satisfying the charge-balance argument in part is the change in oxidation state for the copper bound to the thiol permitting additional copper ions to be incorporated. This mixture of oxidation states is consistent with previous research [15,41,42]. This is a hypothesized explanation for the copper enrichment of the film, which was found to be greater than the idealized 1:1 ratio of copper to molecule. Further research is required to focus on the metal–organic interface to better understand the coordination that is driving the assembly of the film.

4. Conclusions

Topographical structure and internal composition of metal–organic coordinated multilayers have been investigated quantitatively as a function of the number of layers deposited to further understand film formation and structure. SPM studies investigating the morphology of films ranging from 0 to 30 layers showed a distinct transition in the structure that occurred around five layers from a conformal coating mimicking the underlying substrate to a material with its own unique structure. During this transition, bright protrusions appear as islands that coalesce with increasing layer deposition. These thin films were the focus of other studies that examined the film composition with XPS finding them to be copper deficient [44,45]. Here, RBS studies enabled the composition to be studied for thicker films that cannot be probed by XPS, finding the thicker films to be copper enriched. This compositional

difference for the thinner *versus* thicker films mirrors the topographical transition that has been observed herein. RBS also revealed that the molecular density of each layer within the multilayer film is remarkably similar to that of a self-assembled monolayer, indicating a robust and stable structure.

Future work will investigate the effect of the substrate quality and molecular length of organic component on the resulting multilayer film structure and composition. Further analysis of SPM images is underway to glean insights into the intricacies of the film formation, focusing on the morphological transition due to the appearance, growth, and coalescence of islands. The changing roughness of the film will be more extensively studied as well as the effect of heating the sample to anneal the film for improved structural quality. The multilayers studied here serve as a model system for future studies of other metal–organic coordinated thin films with technological applications, such as metal–organic coordinated frameworks.

Acknowledgement

The authors acknowledge funding from NSF grants for the scanning probe microscope (MRI-1126462) and accelerator facility (MRI-0319523 and RUI-0969058). Additional funding was provided by Hope College start-up funds, Nyenhuis Student–Faculty Cooperative Research Grant, and Towsley Scholar Research Award. We thank Prof. Jennifer Hampton and Mr. David Daugherty for technical assistance.

References

[1] L. Netzer, J.A. Sagiv, New approach to construction of artificial monolayer assemblies, J. Am. Chem. Soc. 105 (1983) 674–676.
[2] G. Decher, Fuzzy nanoassemblies: toward layered polymer multicomposites, Science 277 (1997) 1232–1237.
[3] S.L. Clark, P.T. Hammond, Engineering the microfabrication of layer-by-layer thin films, Adv. Mater. 10 (1998) 1515–1519.
[4] O. Shekhah, H. Wang, S. Kowarik, F. Schreiber, M. Paulus, M. Tolan, C. Sternemann, F. Evers, D. Zacher, R.A. Fischer, C. Wöll, Step-by-step route for the synthesis of metal–organic frameworks, J. Am. Chem. Soc. 129 (2007) 15118–115119.
[5] M. Wanunu, A. Vaskevich, S.R. Cohen, H. Cohen, R. Arad-Yellin, A. Shanzer, I. Rubinstein, Branched coordination multilayers on gold, J. Am. Chem. Soc. 127 (2005) 17877–17887.
[6] C.F. Faulkner, R.E. Fischer, G.K. Jennings, Surface-initiated polymerization of 5-(perfluoro-n-alkyl)norbornenes from gold substrates, Macromolecules 43 (2010) 1203–1209.
[7] R. Tao, M. Anthamatten, Condensation and polymerization of supersaturated monomer vapor, Langmuir 28 (2012) 16580–16587.
[8] P.T. Hammond, Form and function in multilayer assembly: new applications at the nanoscale, Adv. Mater. 16 (2004) 1271–1293.
[9] S. Colak, G.N. Tew, Dual-function ROMP-based betaines: effect of hydrophilicity and backbone structure on nonfouling properties, Langmuir 28 (2012) 666–675.
[10] H.F. Chuang, R.C. Smith, P.T. Hammond, Polyelectrolyte multilayers for tunable release of antibiotics, Biomacromolecules 9 (2008) 1660–1668.
[11] J.M. Jensen, A.B. Oelkers, R. Toivola, D.C. Johnson, X-ray reflectivity characterization of ZnO/Al_2O_3 multilayers prepared by atomic layer deposition, Chem. Mater. 14 (2002) 2276–2282.
[12] M. Szot, K. Dybko, P. Dziawa, L. Kowalczyk, E. Smajek, V. Domukhovski, B. Taliashvili, P. Dluzewski, A. Reszka, B.J. Kowalski, M. Wiater, T. Wojtowicz, T. Story, Epitaxial zinc-blende CdTe antidots in rock-salt PbTe semiconductor thermoelectric matrix, Cryst. Growth Des. 11 (2011) 4794–4801.
[13] H. Wang, S. Ishihara, K. Ariga, Y. Yamauchi, All-metal layer-by-layer films: bimetallic alternate layers with accessible mesopores for enhanced electrocatalysis, J. Am. Chem. Soc. 134 (2012) 10819–10821.
[14] W.K. Bae, J. Kwak, J. Lim, D. Lee, M.K. Nam, K. Char, C. Lee, S. Lee, Multicolored light-emitting diodes based on all-quantum-dot multilayer films using layer-by-layer assembly method, Nano Lett. 10 (2010) 2368–2373.
[15] S.D. Evans, A. Ulman, K.E. Goppert-Berarducci, L.J. Gerenser, Self-assembled multilayers of ω-mercaptoalkanoic acids: selective ionic interactions, J. Am. Chem. Soc. 113 (1991) 5866–5868.
[16] H. Lee, L.J. Kepley, H.-G. Hong, S. Akhter, T.E. Mallouk, Adsorption of ordered zirconium phosphonate multilayer films on silicon and gold surfaces, J. Phys. Chem. 92 (1988) 2597–2601.
[17] H.C. Yang, K. Aoki, H.-G. Hong, D.D. Sackett, M.F. Arendt, S.-L. Yau, C.M. Bell, T.E. Mallouk, Growth and characterization of metal (II) alkanebisphosphonate multilayer thin films on gold surfaces, J. Am. Chem. Soc. 115 (1993) 11855–11862.
[18] M.A. Ansell, E.B. Cogan, C.J. Page, Coordinate covalent cobalt–diisocyanide multilayer thin films grown one molecular layer at a time, Langmuir 16 (2000) 1172–1179.
[19] M.A. Ansell, E.B. Cogan, G.A. Neff, R. von Roeschlaub, C.J. Page, Self-assembly of thin film superstructures based on alternating metal–bisphosphonate and cobalt–diisocyanide layers, Supramol. Sci. 4 (1997) 21–26.
[20] S. Bharathi, M. Nogami, S. Ikeda, Layer by layer self-assembly of thin films of metal hexacyanoferrate multilayers, Langmuir 17 (2001) 7468–7471.
[21] A. Hatzor, T. van der Boom-Moav, S. Yochelis, A. Vaskevich, A. Shanzer, I. Rubinstein, A metal–ion coordinated hybrid multilayer, Langmuir 16 (2000) 4420–4423.
[22] D.M. Sarno, B. Jiang, D. Grosfeld, J.O. Afriyie, L.J. Matienzo, W.E. Jones Jr., Self-assembled molecular architectures on surfaces: new strategies involving metal–organic copolymers, Langmuir 16 (2000) 6191–6199.
[23] O. Shekhah, H. Wang, T. Strunskus, P. Cyganik, D. Zacher, R. Fischer, C. Wöll, Layer-by-layer growth of oriented metal organic polymers on a functionalized organic surface, Langmuir 23 (2007) 7440–7442.
[24] H.E. Katz, M.L. Schilling, C.E.D. Chidsey, T.M. Putvinski, R.S. Hutton, Quaterthiophenediphosphonic acid (QDP): a rigid, electron-rich building block for zirconium-based multilayers, Chem. Mater. 3 (1991) 699–703.
[25] S. Richter, C.H.-H. Traulsen, T. Heinrich, J. Poppenber, C. Leppich, M. Hozweber, W.E.S. Unger, C.A. Schalley, Sequence programmable multicomponent multilayers of nanometer-sized tetralactam macrocycles on gold surfaces, J. Phys. Chem. C 117 (2013) 18980–18985.
[26] A.C. Zeppenfeld, S.L. Fiddler, W.K. Ham, B.J. Klopfenstein, C.J. Page, Variation of layer spacing in self-assembled hafnium-1,10-decanediylbis(phosphonate) multilayers as determined by ellipsometry and grazing angle X-ray diffraction, J. Am. Chem. Soc. 116 (1994) 9158–9165.
[27] H. Zhou, S.F. Bent, Molecular layer deposition of functional thin films for advanced lithographic patterning, ACS Appl. Mater. Interfaces 3 (2011) 505–511.
[28] A.V. Walker, Building robust reliable molecular constructs: patterning, metallic contacts, and layer-by-layer assembly, Langmuir 26 (2010) 13778–13785.
[29] A. Hatzor, P.S. Weiss, Molecular rulers for scaling down nanostructures, Science 291 (2001) 1019–1020.
[30] M.E. Anderson, L.P. Tan, M. Mihok, H. Tanaka, M.W. Horn, G.S. McCarty, P.S. Weiss, Photolithographic structures with precise controllable nanometer-scale spacings created by molecular rulers, Adv. Mater. 18 (2006) 1020–1022.
[31] C. Srinivasan, J.N. Hohman, M.E. Anderson, P.S. Weiss, M.W. Horn, Sub-30-nanometer patterning on quartz for nanolithography imprint templates, Appl. Phys. Lett. 93 (2008) 083123–083125.
[32] M.E. Anderson, L.P. Tan, H. Tanaka, M. Mihok, H. Lee, M.W. Horn, P.S. Weiss, Advances in nanolithography using molecular rulers, J. Vac. Sci. Technol. B 21 (2003) 3116–3119.
[33] M.E. Anderson, R.K. Smith, Z.J. Donhauser, A. Hatzor, P.A. Lewis, L.P. Tan, H. Tanaka, M.W. Horn, P.S. Weiss, Exploiting intermolecular interactions and self-assembly for ultrahigh resolution nanolithography, J. Vac. Sci. Technol. B 20 (2002) 2739–2744.
[34] C. Srinivasan, M.E. Anderson, R. Jayaraman, P.S. Weiss, M.W. Horn, Electrically isolated nanostructures fabricated using self-assembled multilayers and a novel bi-layer resist stack, Microelectron. Eng. 83 (2006) 1517–1520.
[35] S. Pookpanratana, J.W.F. Robertson, C. Jaye, D.A. Fischer, C.A. Richter, C.A. Hacker, Electrical and physical characterization of bilayer carboxylic acid-functionalized molecular layers, Langmuir 29 (2013) 2083–2091.
[36] H.-G. Hong, T.E. Mallouk, Electrochemical measurements of electron transfer rates through zirconium 1,2-ethanediylbis(phosphonate) multilayer films on gold electrodes, Langmuir 7 (1991) 2362–2369.
[37] H.E. Katz, M.L. Schilling, Electrical properties of multilayers based on zirconium phosphate/phosphonate bonds, Chem. Mater. 5 (1993) 1162–1166.
[38] M. Altman, A.D. Shukla, T. Zubkov, G. Evmenenko, P. Dutta, M.E. van der Boom, Controlling structure from the bottom-up: structural and optical properties of layer-by-layer assembled palladium coordination-based multilayers, J. Am. Chem. Soc. 128 (2006) 7374–7382.
[39] G.A. Neff, M.R. Helfrich, M.C. Clifton, C.J. Page, Layer-by-layer growth of acentric multilayers of Zr and azobenzene bis(phosphonate): structure, composition, and second-order nonlinear optical properties, Chem. Mater. 12 (2000) 2363–2371.
[40] M. Brust, P.M. Blass, A.J. Bard, Self-assembly of photoluminescent copper(I)-dithiol multilayer thin films and bulk materials, Langmuir 13 (1997) 5602–5607.
[41] T.L. Freeman, S.D. Evans, A. Ulman, XPS studies of self-assembled multilayer films, Langmuir 11 (1995) 4411–4417.
[42] A.W. Czanderna, D.E. King, D. Spaulding, Metal overlayers on organic functional groups of self-organized molecular assemblies. 1. X-ray photoelectron spectroscopy of interactions of Cu/COOH on 11-mercaptoundecanoic acid, J. Vac. Sci. Technol. A 9 (1991) 2607–2613.
[43] C.M. Whelan, J. Ghijsen, J.-J. Pireaux, K. Maex, Cu adsorption on carboxylic acid-terminated self-assembled monolayers: a high-resolution X-ray photoelectron spectroscopy study, Thin Solid Films 464–465 (2004) 388–392.
[44] T.A. Daniel, S. Uppili, G. McCarty, D.L. Allara, Effects of molecular structure and interfacial ligation on the precision of Cu-bound α, ω-mercaptoalkanoic acid "molecular ruler" stacks, Langmuir 23 (2007) 638–648.
[45] S. Johnson, J. Chan, D. Evans, A.G. Davies, C. Wälti, Effect of chain length on the assembly of mercaptoalkanoic acid multilayer films ligated through divalent Cu ions, Langmuir 27 (2011) 1033–1037.
[46] S. Johnson, A. Bronowska, J. Chan, D. Evans, A.G. Davies, C. Wälti, Redox-induced conformational change in mercaptoalkanoic acid multilayer films, Langmuir 28 (2012) 6632–6637.
[47] J.R. Bird, J.S. Williams, Ion Beam for Materials Analysis, Academic Press, Australia, 1989.
[48] S.A.E. Johansson, J.L. Campbell, K.G. Malmqvist, Particle-Induced X-ray Emission Spectrometry (PIXE), Wiley, New York, 1995.
[49] J.A. Maxwell, W.J. Teesdale, J.L. Campbell, The Guelph PIXE software package II, Nucl. Instr. Meth. B95 (1995) 407–421.

[50] M. Mayer, SIMNRA User's Guide, Report IPP 8/113, Max-Planck-Institut für Plasmaphysik, 1997. (Garching, Germany).
[51] M. Mayer, SIMNRA, a simulation program for the analysis of NRA, RBS and ERDA, AIP Conf. Proc. 475 (1999) 541–544.
[52] S. Huo, W. Schwarzacher, Anomalous scaling of the surface width during Cu electrodeposition, Phys. Rev. Lett. 86 (2001) 256–259.
[53] M.C. Lafouresse, P.J. Heard, W. Schwarzacher, Anomalous scaling for thick electrodeposited films, Phys. Rev. Lett. 98 (2007) 2361011–2361014.
[54] D. Kirkwood, V.C. Zoldan, A.A. Pasa, G. Zangari, Evolution of surface-roughness in electrodeposited Co–Ni–P and Co–Ni films, J. Electrochem. Soc. 157 (2010) D181–D186.
[55] R.C. Weast, CRC Handbook of Chemistry and Physics, 69th ed. CRC Press, Boca Raton, FL, 1988.
[56] J.C. Love, L.A. Estroff, J.K. Kriebel, R.G. Nuzzo, G.M. Whitesides, Self-assembled monolayers of thiolates on metals as a form of nanotechnology, Chem. Rev. 105 (2005) 1103–1170.